University of Huddersfield Repository

Stejskal, Lenka

Structural characterisation of outer membrane proteins from Borrelia burgdorferi sensu lato by small-angle X-ray scattering

Original Citation

This version is available at http://eprints.hud.ac.uk/26728/

http://eprints.hud.ac.uk/

Structural characterisation of outer membrane proteins from *Borrelia burgdorferi sensu lato* by small-angle X-ray scattering

Lenka Stejskal
Email: U1068440@unimail.hud.ac.uk

Abstract

Forming the interface between the bacterial cell and the host, the outer membrane of Borrelia is known to play a key role in pathogenicity. Although *Borrelia burgdorferi sensu lato* are considered to be Gram-negative, their outer membrane is unique, lacking liposaccharides and phosphatidylethanolamine. It contains a variety of glycolipids, surface exposed lipoproteins and a number of membrane-spanning β-barrels. BAPKO_0422, BB_0562 and BG_0408 are membrane proteins, theoretically predicted to form 8-stranded, membrane-spanning β-barrels. The aim of this work is to produce recombinant versions of these proteins, and determine molecular envelopes by small-angle X-ray scattering (SAXS). The β-barrel model can then be tested by comparing the experimental molecular envelope with the theoretical predictions.

Three Borrelia proteins (BAPKO_0422, BB_0562 and BG_0408) were recombinantly expressed in the *E. coli* expression system using the pET-47 expression vector. The putative membrane proteins were purified by immobilised metal affinity chromatography (IMAC). The His tag of BAPKO_0422 was enzymatically removed to produce a native protein, and to allow for a visual comparison of the protein both with and without the His tag.

SAXS data for each protein were collected and the overall shape was determined using *ab initio* methods. The pair-distance distribution function (*P(r)* function) of BAPKO_0422 with the His tag indicated a particle overlap potentially caused by the flexible 6-His tag at the N-terminus. Kratky plots of BAPKO_0422, BB_0562 and BG_0408 revealed the parabolic convergence for a folded particle.

The low-resolution molecular envelopes of BAPKO_0422, BB_0562 and BG_0408 are consistent with the structure of an 8-stranded β-barrel. The filtered envelopes are in agreement with the shape and size of the *E. coli* homologue OmpX. The likely orientation of the protein within the outer membrane can be deduced by comparing molecular envelopes with and without the N-terminal His tag. The data suggest that BAPKO_0422, BB_0562 and BG_0408 are single-domain cylindrical-shaped molecules with no evidence of an internal pore. Several questions remain to be answered, such as the oligomeric state of BG_0408 and BAPKO_0422. The function of these 8-stranded β-barrels in the *Borrelial* outer membrane remains to be investigated.

Keywords: *Borrelia;* outer membrane proteins; Lyme disease; spirochetes; β-barrel; small-angle X-ray scattering; factor H.

Introduction

Lyme disease

Lyme disease, also known as Lyme *borreliosis*, is a zoonotic infection transmitted to humans from the mid-gut of Ixodic ticks infested with the group of spirochetal bacteria *Borrelia burgdorferi sensu lato* (Steere, 2001). It is now the most common vector-borne disease in the Northern Hemisphere (Lindgren & Jaenson, 2006). There are 19 species collectively referred to as *Borrelia burgdorferi sensu lato*, and four are currently known to be human pathogens: *Borrelia burgdorferi*, *Borrelia garinii*, *Borrelia afzelii* and *Borrelia miyamotoi* (Rudenko, Golovchenko, Belfiore, Grubhoffer, & Oliver, 2014). These spirochetes are commonly found in nature in sylvatic cycles comprising of ticks of the *Ixodes ricinus* complex and a variety of mammals and migratory birds. The main vectors of the human infection are deer ticks *Ixodes scapularis* and *pacificus* in the USA, the sheep tick *Ixodes ricinus* and taiga tick *Ixodes persulcatus* in Europe, and the latter also in Asia (Steere, Coburn, & Glickstein, 2004). Up to 80% of Ixodic ticks are reported to be infected with *Borrelia burgdorferi sensu lato* in highly endemic areas (Barbour, 1998).

The first and most common clinical manifestation of Lyme *borreliosis* in approximately 80% of cases is erythema migrans (EM), a cutaneous lesion annularly expanding around the site of a tick bite appearing several days to weeks after the event (Stanek et al., 2011). Without a suitable treatment, spirochete dissemination to other tissues via the bloodstream may occur and EM can develop at various sites across a body (Stanek et al., 2011). Acute neuroborreliosis appears in about 10–15% of untreated patients, with symptoms such as facial palsy, meningitis and, on rare occasions, cardiac manifestations (Auwaerter, Aucott, & Dumler, 2004). Involvement of the musculoskeletal system, firstly restricted to the muscle and large joint adjacent to the bite site, is often observed. If these rheumatic and neurological symptoms persist, the disease is classed as chronic (late) Lyme *borreliosis* (Biesiada, Czepiel, Lesniak, Garlicki, & Mach, 2012).

Cell structure of Borrelia

Borrelia are tightly coiled and greatly motile bacteria that, like other spirochetes, consists of a protoplasmic cylinder, a peptidoglycan-cytoplasmic membrane complex, a flagellum and a periplasmic space confined by the outer membrane lipid bilayer (Radolf et al., 1995). Interestingly, the flagella filaments are not located at the outer membrane as they are for most bacteria, but are inserted at the termini of the protoplasmic cylinder (Barbour & Hayes, 1986) and fully contained within the periplasmic space (Radolf, Caimano, Stevenson, & Hu, 2012). It is the rotation of these flagella that drives the left-handed corkscrew movement characteristic of *Borrelia* (Kudryashev, Cyrklaff, Wallich, Baumeister, & Frischknecht, 2010).

Because of its double-membrane, *Borrelia* is considered to belong to the Gram-negative group of bacteria. Genetic analyses and ultrastructural and molecular studies, however, have identified a wide taxonomic gap between *Borrelia* and other Gram-negative bacteria and suggested that the spirochetes are likely to form a separate eubacterial phylum (Paster et al., 1991).

Unusual structure of the Borrelia outer membrane

The outer membrane of *Borrelia* is very fluid and consists of 3–4% carbohydrates, 23–50% lipids and 45–62% proteins (Barbour & Hayes, 1986). It differs from other

Gram-negative bacteria in its lack of liposaccharide (LPS) and phosphatidylethanolamine (PE) (Radolf et al., 2012). Since the LPS is highly antigenic, it has been suggested that its absence is at least partially responsible for the immune system evasion (Seemanapalli, Xu, McShan, & Liang, 2010). The main lipid components of the membrane are phosphatidylcholine (PC) and phosphatidylglycerol (PG), both of which are not commonly found in the outer membrane of any other proteobacteria (Radolf et al., 2012). Three glycolipids can be found in *Borrelia*, two of which contain cholesterol: cholesteryl-6-*O*-acyl-β-D-galactopyranoside (ACGal), cholesteryl-β-D-galactopyranoside (βCGal) and mono-α-galactosyl-diacylglycerol (MGalD) (LaRocca et al., 2010). Lipoproteins, such as decorin-binding proteins and outer surface proteins (Osps), are greatly expressed by *Borrelia* and are anchored to the outer membrane by lipidation.

In fact, no other bacteria is known to possess such a large number of lipoproteins in the outer membrane (Templeton, 2004). Unlike in other Gram-negative bacteria, it is the cytoplasmic membrane rather than the outer membrane that is closely associated with the peptidoglycan cell wall. This results in a significant instability of the outer membrane, and the means by which it remains intact is not known (Cullen, Haake, & Adler, 2004).

The uniqueness of the *Borrelia* outer membrane is further enhanced by the evidence of free cholesterol and cholesterol esters (LaRocca et al., 2010), usually only found in eukaryotic cells and a small number of prokaryotes. Recently, the formation of cholesterol-rich lipid rafts never seen in a prokaryotic cell and its association with OspA, OspB and putative β-barrel outer membrane protein P66 was documented (LaRocca et al., 2013).

Structure of β-barrel proteins
β-barrels are outer-membrane-spanning proteins found in Gram-negative bacteria, chloroplasts and mitochondria (Schulz, 2000). They form supersecondary structures composed of between 8 and 24 anti-parallel β-strands that twist and coil to form closed barrel structures with the lumen being transverse to the surface of the outer membrane. In Gram-negative bacteria, they can be arranged into six families, depending on their function (Table 1). Every β-strand is laterally bonded to the next by anti-parallel hydrogen bonds and the first N-terminal β-strand is bonded to the last C-terminal β-strand (Freeman, Landry, & Wimley, 2011; Murzin, Lesk, & Chothia, 1994). Only approximately 10 residues of alternating polar and non-polar amino acids form into the trans-membrane β-strand and span the outer membrane, which hinders the identification of OMPs from the sequence data (Freeman et al., 2011).

Family	Function	Examples
I.	Porins	OmpC, OmpF and PhoE
II.	Passive transporters	LamB, ScrY and FadL
III.	Active transporters	FepA, FecA and FhuA
IV.	Enzymes	phospholipase OmpLA protease OmpT
V.	Defensive proteins	OmpX
VI.	Structural proteins	OmpA

Table 1. Functional groups of outer membrane proteins. Outer membrane proteins divided into families according to their function (Tamm, Hong, & Liang, 2004).

The principles of a β-barrel fold

The construction rules were set out by Schulz (2000). The N and C termini are both located at the periplasmic side of the barrel. The number of β-strands is even, one exception being the 19-stranded VDAC channel in mitochondria (Maurya & Mahalakshmi, 2013) and chloroplasts membrane (Hayat & Elofsson, 2012). The tilt of the β-strand is around 45° and resembles the β-sheet twist. Although two tilt orientations are possible, only one is energetically favoured. When n equals the number of β-strands, the shear number of a β-barrel is normally $n + 2$. Every β-strand is anti-parallel to its adjacent strand and connected to it by hydrogen bonds. At the periplasmic end, β-strands are connected to each other by short turns consisting of a couple of residues called T1, T2, T3, etc. At the external barrel end, β-strands are connected to each other by long loops numbered L1, L2, L3, etc. Side chains of non-polar residues are at the surface of the β-barrel and in direct contact with the outer membrane. Around this hydrophobic part of the β-barrel, two girdles of aromatic side chains contact the non-polar-polar interface of the membrane. In comparison with soluble proteins, the evolutionary sequence variability of β-barrels, particularly that of the external loops, is high and the loops are relatively mobile.

β-barrels in E. coli

OmpA

Arguably the most widely studied β-barrel protein is the 8-stranded outer membrane protein A (OmpA) in *E. coli* (Pautsch & Schulz, 2000). OmpA is a 35 kDa protein and its trans-membrane domain is greatly conserved among Gram-negative bacteria (Prasadarao et al., 1996). It comprises two domains: 154 amino acid residues form the globular periplasmic C-terminal domain and 171 residues fold into the β-barrel membrane-spanning N-terminal domain (Wu et al., 2013). The C-terminal domain is located in the periplasm and connects the peptidoglycan cell wall to the outer membrane (Wang, 2002). OmpA is highly expressed and is heavily regulated at the post-translational level (Smith, Mahon, Lambert, & Fagan, 2007). It is a multifunctional protein playing its role in the structural integrity of the membrane (Prasadarao et al., 1996), acting as a receptor for various bacteriophages and mediating bacterial-host pathogenesis (Smith et al., 2007).

OmpW and OmpX

OmpW and OmpX belong to the same family of small outer membrane proteins that are highly preserved among the Gram-negative bacteria (Hong, Patel, Tamm, & Van Den Berg, 2006; Vogt & Schulz, 1999). OmpX is a single-domain 18 kDa protein

(Vogt & Schulz, 1999) and is thought to be a mediator of bacteria-host adhesion and part of a bacterial defence against the complement immune system (Fernández et al., 2001). Owing to the lack of a pathway between the periplasmic and external side of the β-barrel, OmpX is not likely to act as a pore (Vogt & Schulz, 1999).

OmpW is a 21 kDa single-domain protein (Pilsl, Smajs, & Braun, 1999) and, in contrast with OmpX, is thought to function as a hydrophobic channel (Hong et al., 2006). It has been recently reported that OmpW helps to protect *E. coli* against host phagocytosis. Its expression is regulated by iron, and it was therefore suggested that this immune resistance may play a significant role in iron-related diseases (Wu et al., 2013).

β-barrels in the Borrelial outer membrane
In contrast to many lipoproteins, only a few integral outer membrane proteins are currently known to be present in *Borrelia:* 22 or 24 β-stranded P66 (Kenedy et al., 2014), 16 β-stranded BamA (Noinaj et al., 2013), 16 β-stranded BesC (Bunikis et al., 2008) and 14–16 β-stranded DipA (Thein et al., 2012). The density of OMPs in the outer membrane is reported to be approximately 10-fold lower than of that in *E.coli* (Lenhart & Akins, 2010). BamA, owing to its homology to the β-barrel assembly machine (BAM) protein complex in *E. coli* responsible for the folding and orientation of outer membrane proteins, is thought to orchestrate the assembly of β-barrel proteins in the *Borrelial* outer membrane (Lenhart & Akins, 2010).

BAPKO_0422 and other 8-stranded β-barrels
The recent discovery of a functional *β*-barrel-assembly apparatus in *Borrelia* (Lenhart & Akins, 2010) suggests that a range of other β-barrel proteins are likely to exist in the outer membrane, analogous to other Gram-negative bacteria. As the OmpA-like membrane-spanning domain (PFAM database – PF01389) is highly conserved among other diderm bacteria, it is possible that similar 8-stranded β-barrels are also present in *Borrelia*. Bioinformatic analysis of the *Borrelial* genome (Dyer, Brown, Stejskal, Laity, & Bingham, 2015) identified several such candidate proteins, including BAPKO_0422, BAPKO_0026, BG_0027, BG_0407, BB_0562, BB_0406 and BG_0408, that are likely to form 8-stranded β-barrels in *Borrelia burgdorferi sensu lato*. BAPKO_0422, BB_0562, BG_0408 and BB_0406 were successfully cloned into a pET-47b(+) plasmid and expressed in an *E. coli* expression system. The recombinant proteins will be purified and structurally characterised by SAXS.

Methodology
Expression of recombinant proteins from E. coli
Lysogeny broth (containing 50 mg/L kanamycin and 34 mg/L chloramphenicol) was inoculated with an overnight culture of Rosseta™ *E. coli* cells containing a pET-47b(+) (Novagen) construct with BAPKO_0422, BB_0562 or BG_0408 coding sequences fused to an N-terminal 6x-His tag. The flasks were placed at 37℃ with shaking at 120 rpm for 3 hours. Protein expression was induced at an O.D. of 0.6 by addition of IPTG stock solution to a final concentration of 1 mM. The cultures were then left at 37℃/120 rpm for 4 hours, and transferred to 4℃/50 rpm and left overnight. The cultures were then centrifuged at 4℃, 10,000G for 10 minutes. The pellets containing inclusion bodies with the proteins of interest were kept for protein purification.

Protein purification
Borrelial outer membrane proteins
The pellets containing inclusion bodies were re-suspended in 0.3 M NaCl, 50 mM Tris, pH 8 (10 ml per gram wet weight of cells), placed on ice and sonicated at 95% amplitude with 5 seconds on and 10 seconds off intervals for 5 minutes. The lysate was centrifuged at 4°C, 20,000G for 1 hour and the pellet was then re-suspended in 0.3 M NaCl, 50 mM Tris-HCl, 10 mM EDTA, 10 mM DTT, 0.5% (w/v) Triton x 100, pH 8 and centrifuged at 4°C, 10,000G for 15 minutes. This was repeated twice. The pellet was then washed with 0.3 M NaCl, 50 mM Tris, pH 8 twice and re-suspended in 8 M urea, 0.3 M NaCl, 50 mM Tris-HCl, pH 8, left in a fridge for 4 days and centrifuged at 4°C, 10,000G for 30 minutes. The supernatant was kept for further purification by IMAC.

IMAC
Borrelial outer membrane proteins
The His-Trap HP 5 ml column (GE Healthcare) and FPLC system were equilibrated using 10 column volumes (CV) of 8 M urea, 0.3 M NaCl, 50 mM Tris-HCl, pH 8 at speed 5 ml/min. The supernatant was loaded at speed 0.5 ml/min with an additional 20 ml of the buffer. Proteins were refolded by running a gradient over 15 CV into 0.3 M NaCl, 50 mM Tris-HCl, 1 M urea, pH 8 buffer. Non-specifically bound proteins were eluted using 50 ml of 0.3 M NaCl, 50 mM Tris-HCl, 20 mM imidazole, 0.1% (w/v) LDAO, pH 8 at speed 5 ml/min. *Borrelial* proteins were eluted using 0.3 M NaCl, 50 mM Tris-HCl, 0.3 M imidazole, 0.1% (w/v) LDAO, pH 8 buffer at speed 5 ml/min.

Enzymatic removal of 6x-His tag
Purified BAPKO_0422 was transferred to an Amicon Ultra-15 Centrifugal Filter Units™ (Fisher) and centrifuged at 4°C, 5,000G for 20 minutes and concentrated to 3.5 mg/ml. Protein concentration was determined by measuring the absorbance at 280 nm. LDAO was added into HRV-3C protease to make the total LDAO concentration 0.1% (w/v). Enzyme digests were carried out with an excess of BAPKO_0422 at a ratio of 50:1, 20:1 and 10:1 and then incubated at 4°C under gentle agitation for 2 days.

Purification of BAPKO_0422 digest by IMAC

The mixture of BAPKO_0422 and HRV-3C protease obtained after digest was loaded onto the His-Trap HP 5 ml column at speed 0.5 ml/min after the systems were equilibrated using 10 CV of 8 M urea, 0.3 M NaCl, 50 mM Tris-HCl, pH 8 at speed 5 ml/min. The non-bound BAPKO_0422 was then collected. The bound HRV-3C protease was eluted using 50 ml of 0.3 M NaCl, 50 mM Tris-HCl, 0.3 M imidazole, pH 8.

Extended dialysis
His-Trap column purification of OMPs and the digested BAPKO_0422 were transferred into Amicon Ultra-15 Centrifugal Filter Units™ and concentrated to 250 µl. Proteins were injected into Dialysis Cassette Slide-A-Lyzer™ using a syringe and 18 gauge needle (Fisher) and were then dialysed against 200 ml of 0.3 M NaCl, 50 mM Tris-HCl, 0.1% (w/v) LDAO, 0.05% sodium azide, pH 8 for 5 days. Samples of dialysis buffer were stored at –20°C for use as a matched blank for SAXS.

SDS-PAGE analysis

The samples contained between 20 and 50 μg of protein. For the boiled SDS-PAGE, 2 μl of DTT was added and the samples were boiled at 70°C for 10 minutes. Samples were loaded onto pre-cast 4–12 % (w/v) Bis/Tris gels (Invitrogen) with 10 μl of Novex Sharp Pre-stained protein standards (Invitrogen). Gels were run at 150 kV, 140 mA for 60–90 minutes.

SAXS

Data collection

The dialysed sample was centrifuged at 4°C, 10 ,000G for 1 hour. Protein concentration was determined by measuring the absorbance at 280 nm. SAXS data was acquired using a Bruker Nanostar from 100 μl solutions of BAPKO_0422 (2.8 and 3.5 mg/ml), BB_0562 (3 mg/ml) and BG_0408 (4.2 mg/ml) in 0.3 M NaCl, 50 mM Tris-HCl, 0.1% (w/v) LDAO, 0.05% sodium azide, pH 8. The distance of the sample and the detector was set to 106.850 cm. Samples were exposed to X-rays for 2,400 seconds, resulting in between 250,000 and 350,000 counts per image. A full data set consisted of 10 images of the sample at 2,400 seconds each (24,000 seconds in total). Full data sets were also collected from blank samples to enable subtraction of ambient scattering. After extended dialyses, 100 μl of dialysis buffer was kept and used as a matched blank. This scattering data was then integrated using the circular integration method (rotation around Chi) to obtain a scattering curve.

Primus software (ATSAS) (Petoukhov et al., 2012) was then used to take the average of the 10 scattering curves from both sample and blank, and the blank was subtracted.

Data analysis

Guinier and Kratky plots were generated in Primus software. GNOM (ATSAS) (Petoukhov et al., 2012) was used to generate the *P(r)* function (pair-distance distribution function).

Ab initio shape determination using dummy atoms was performed using the online ATSAS package (Petoukhov et al., 2012) with default settings. DAMMIN generated 20 models, which were then aligned by DAMAVER. Outliers were removed and an average model was generated in DAMFILT. Figures were generated in PyMOL (Schrodinger, 2010).

Results

IMAC

Proteins BAPKO_0422, BB_0562 and BG_0408 were harvested from inclusion bodies and purified using Ni-NTA chromatography (Figure. 1). The single peak in the latter half of the trace indicates elution of the target protein (indicated by black arrow).
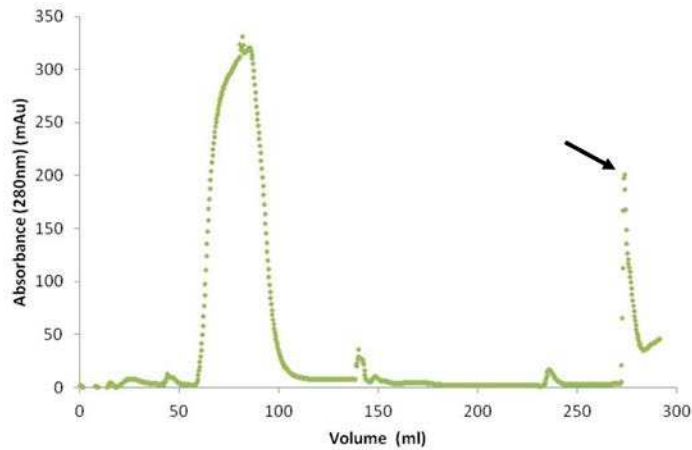
Figure 1. IMAC chromatogram of purification and refolding of BAPKO_0422 from inclusion bodies. Sample was loaded in 8 M urea, 0.3 M NaCl, 50 mM Tris-HCl, pH 8 at speed 0.5 ml/min-1. The large peak from 50 to 100 ml is the loading peak, representing proteins that did not bind to the column. The refold gradient was set over 75 ml. Non-specifically bound proteins were washed with 50 ml of 0.3 M NaCl, 50 mM Tris-HCl, 20 mM imidazole, 0.1% (w/v) LDAO, pH 8 and the small peak can be observed at approximately 230 ml. The peak indicated by the arrow indicates elution of BAPKO_0422.

SDS-PAGE
Lysate, soluble/insoluble fractions and purified protein were analysed by SDS-PAGE to observe the purity and oligomeric state of the recombinant proteins. The purified fraction of BG_0408 revealed multiple bands at 250, 150 and 60 kDa, possibly indicating the formation of multimers (Figure. 2). The purified fraction of BB_0562 (Figure. 3) shows a major band at 25 kDa corresponding the Mw of the tagged protein (Table 2). BAPKO_0422 was purified to homogeneity by Ni-NTA and size exclusion chromatography, and revealed a band of the expected Mw (Dyer et al., 2015).
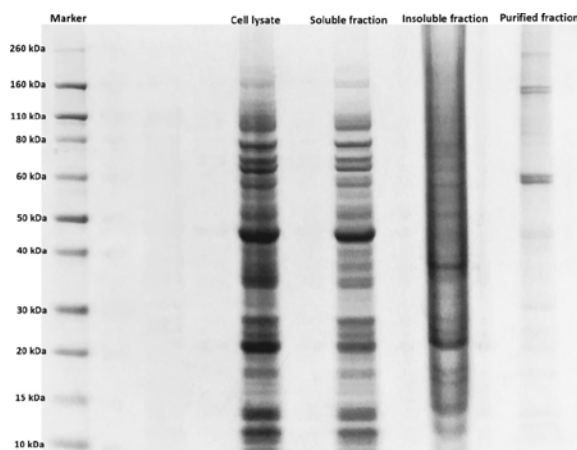

Figure 2. Non-boiled SDS-PAGE of BG_0408 fractions. L–R: 10 µl of Novex Sharp Pre-stained protein standards, 10 µl of cell lysate, 10 µl of soluble fraction, 10 µl of insoluble fraction and 20 µl of purified fraction. Large band at around 45 kDa in the cell lysate and soluble fraction is likely to be an E. coli protein. Two bands at 20 and 38 kDa are visible in the insoluble fraction and the pure fraction shows three bands at 60, 150 and 250 kDa.

Protein	Amino acid sequence of recombinant protein	Molecular weight	UniProt Accession code
BB_0562	MAHHHHHHSAALEVLFQGPGYQDPKDSY LNRGIGFGASIGNPIINLIMSFPFIDFEIGYG GSNGINLSGPKLESKFYDFNLLAIAALDFIF TISLIKNLNLGIGIGGNISISSHTSKLINVELG FGMRIPLVIFYDITENLEIGMKIAPSIEFISN TRSLAQHRTYSGIKSNFAGGIFAKYYIF	20.2 kDa	O51510
BG_0408	MAHHHHHHSAALEVLFQGPGYQDPSDN YMVRCSKEEDSTTCIAKLKGIKEKKSYDLF SMGIGIGNPIANIIITIPYVNIDFGYGGFIGP KSNNFENYLNGGIDIIFKKQIGQYMRIGGG IGIGADWSKTSLMPPDEEEETDYERIGAVI RIPFVMEYNFAKNLYIGFKVYPALGPTILLT KPNILFEGIKFNFFGFGFIKFAFN	22.8 kDa	Q661L3
BAPKO_0422	MAHHHHHHSAALEVLFQGPGYQDPQSK SKTMVEDDFDFEKLLEKEESVRRLFGIGF GIGYPLTNITISVAYVDIDLGYGRFVGLKPN NFMPYVVMGIDLLIKDEIHKNTMISGGIGM GADWSKGSPEKSNENLEGDVNEDQQTS LENRIGVVIRLPLVIEYSFLKNIVIGFKAVAT IGTTMLFGNPMSFEGARFNFLGTGFIKIYI	22.9 kDa	Q0SNA2

Table 2. The sequence and molecular weight of recombinant proteins. The accession codes were obtained from UniProt database (The UniProt Consortium, 2015).
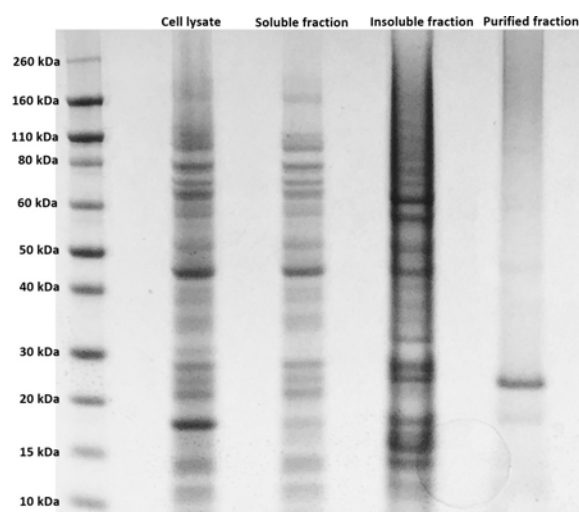

Figure 3. Non-boiled SDS-PAGE of BB_0562 fractions. L–R: 10 µl of Novex Sharp Pre-stained protein standards, 10 µl of cell lysate, 10 µl of soluble fraction, 10 µl of insoluble fraction and 20 µl of purified fraction. The large band at 45 kDa in cell lysate and soluble fraction is likely to be an E. coli protein. The purified fraction shows two bands at 18 and 25 kDa.

SAXS

Instrumental set-up

Nanography was used to ensure that the capillary was centred in the X-ray beam. The sample holder was aligned so the capillary was exposed in line with the centre of the X-ray beam and the centre of the capillary (42.5 × 49 mm) was determined by the coordinates with the fewest number of counts (Figure. 4).
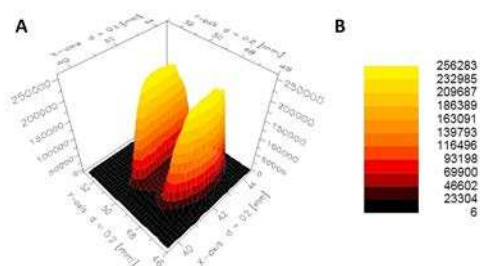

Figure 4. Diagram of Bruker Nanography. a) Central X and Y axis coordinates are 42.5 mm and 49 mm respectively. b) Colour-coded ladder showing number of counts.

X-ray scattering data (Figure. 5) for solutions of BAPKO_0422, BB_0562 and BG_0408 were collected as described in the methodology section. Guinier analysis is useful for assessing the quality of the scattering data. Sample polydispersity can be revealed, and an estimate of the radius of gyration can be calculated from the gradient of the linear region (R_g = sqrt(–3m), where m is the gradient) using the Guinier law. Guinier analysis of the BAPKO_0422, BB_0562 and BG_0408 scattering data revealed a linear region with a small upturn at low q values (Figure. 6). The residual analysis (Figure. 6) indicates a monodisperse solution. The gradient of the linear region was used to calculate R_g values in reciprocal space (Tables 3, 4, 5 and 6).
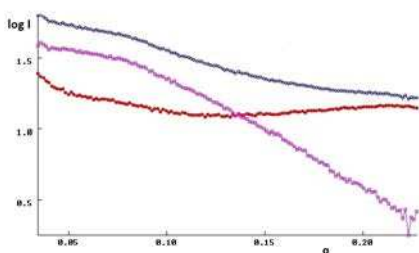

Figure 5. Representative scattering curve of 3.5 mg/ml BAPKO_0422 in solution. Raw scattering data obtained by Primus software (ATSAS) (Petoukhov et al., 2012) showing the log I (relative units) over the scattering vector (q, Å-1) of BAPKO_0422 (blue line), solvent blank (red line) and the BAPKO_0422 with the blank subtracted (purple line).
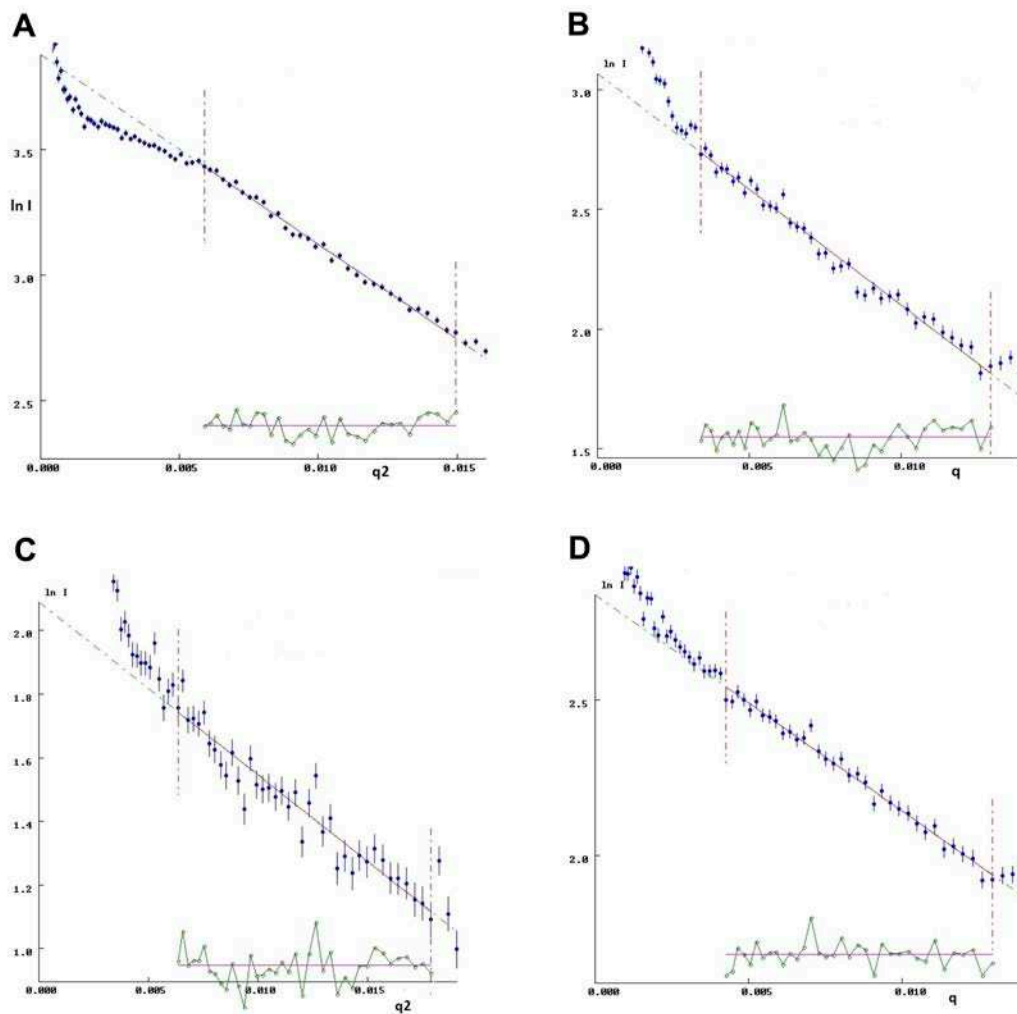
Figure 6. Guinier plots of BAPKO_0422 (A), 6x-His-tagged BAPKO_0422 (B), 6x-His-tagged BB_0562 (C) 6x-His-tagged BG_0408 (D). Guinier plots obtained by Primus software (ATSAS) (Petoukhov et al., 2012) showing the log I (relative units) vs q2 (Ǻ-2) with the corresponding residuals in the lower plot. The indicated linear regions were used to calculate the Rg values shown in Table 3.

R_g value generated using Primus software (ATSAS) for 3.5 mg/ml of BAPKO_0422 in solution	R_g value (Å)
Guinier plot	15.00
GNOM fit - reciprocal space	14.30
P(r) **plot - real space**	14.29

Table 3. Table of 3.5 mg/ml BAPKO_0422 in solution Rg values generated using Primus software (ATSAS) (Petoukhov et al., 2012).

R_g value generated using Primus software (ATSAS) for 2.8 mg/ml of BAPKO_0422 in solution	R_g value (Å)
Guinier plot	17.00
GNOM fit - reciprocal space	16.26
P(r) **plot - real space**	16.29

Table 4. Table of 2.8 mg/ml BAPKO_0422 in solution Rg values generated using Primus software (ATSAS) (Petoukhov et al., 2012).

R_g value generated using Primus software (ATSAS) for 3.0 mg/ml of BB_0562 in solution	R_g value (Å)
Guinier plot	12.80
GNOM fit - reciprocal space	13.28
P(r) **plot - real space**	13.29

Table 5. Table of 3.0 mg/ml BB_0562 in solution Rg values generated using Primus software (ATSAS) (Petoukhov et al., 2012).

R_g value generated using Primus software (ATSAS) for 4.2 mg/ml of BG_0408 in solution	R_g value (Å)
Guinier plot	14.40
GNOM fit - reciprocal space	14.65
P(r) **plot - real space**	14.66

Table 6. Table of 4.2 mg/ml BB_0562 in solution Rg values generated using Primus software (ATSAS) (Petoukhov et al., 2012).
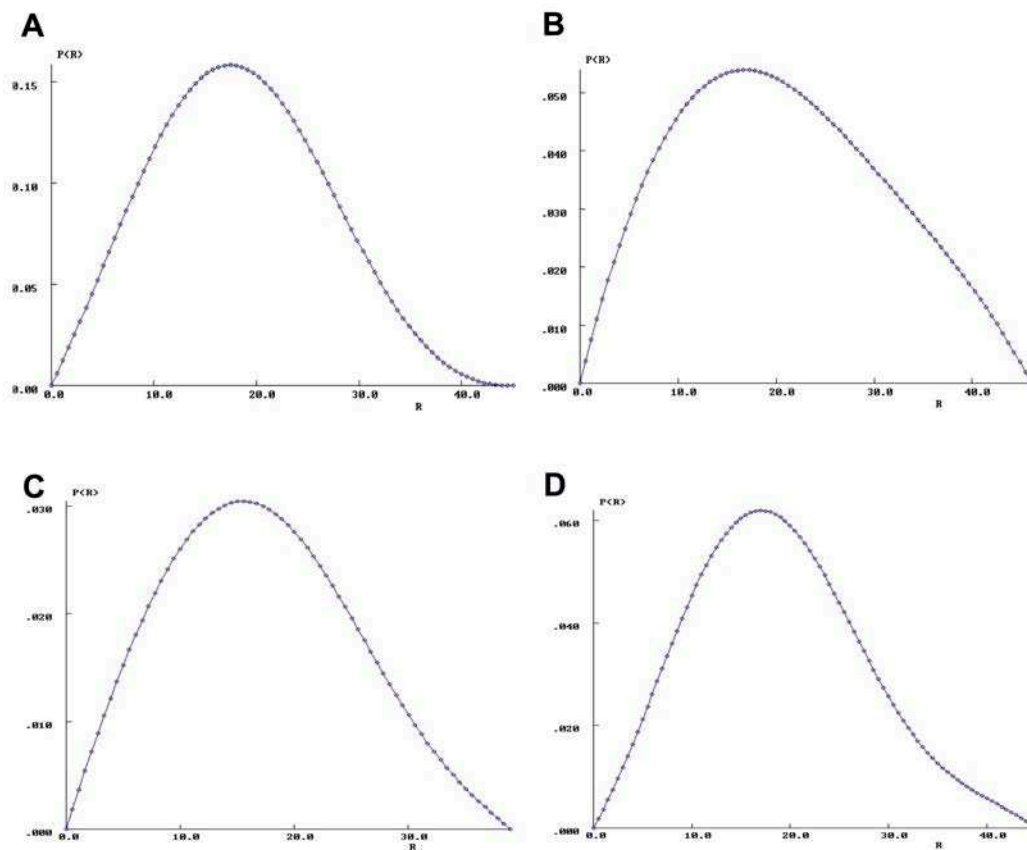
Figure 7. Pair-distribution plots P(r) of BAPKO_0422 (A), 6x-His-tagged BAPKO_0422 (B), 6-xHis-tagged BB_0562 (C) 6x-His-tagged BG_0408 (D). The P(r) plot was obtained through a Fourier transform of the raw scattering data in reciprocal space evaluated by GNOM (ATSAS) (Petoukhov et al., 2012). Pair-distribution function (P(r) vs R, Å-1) was used to obtain the blue bell-shaped curve indicative of a globular single-domain molecule. The P(r) function was used to calculate Rg values in the real space.

The pair-distribution function, *P(r),* is a plot of all possible distances between pairs of electrons within a macromolecule and therefore provides information on the shape of the molecule. Information on interparticle interference (overlap or repulsion) is also available. The *P(r)* functions of BAPKO_0422 (tagged and untagged), BB_0562 and BG_0408 are all indicative of globular, single-domain molecules (Figure. 7). The *P(r)* function of untagged BAPKO_0422 (Figure. 7A) approaches zero at a steady rate, as would be expected for a spherical molecule with well-defined edges. However, the data for 6x-His-tagged BAPKO_0422 (Figure. 7B) and BG_0408 (Figure. 7D) do not approach zero at a steady slope and may be indicative of either interparticle interference or particle overlap, potentially caused by the flexible 6x-His tag at the N-terminus (Jacques & Trewhella, 2010). There is some uncertainty in Dmax from this data.

Kratky plots of BAPKO_0422, BB_0562 and BG_0408 (Figure. 8) revealed the parabolic convergence for a folded particle. The clear peak is indicative of a compact globular folded structure with well-defined difference between the scattering of molecule and solvent. The data reveals that BB_0562 appears to be the most

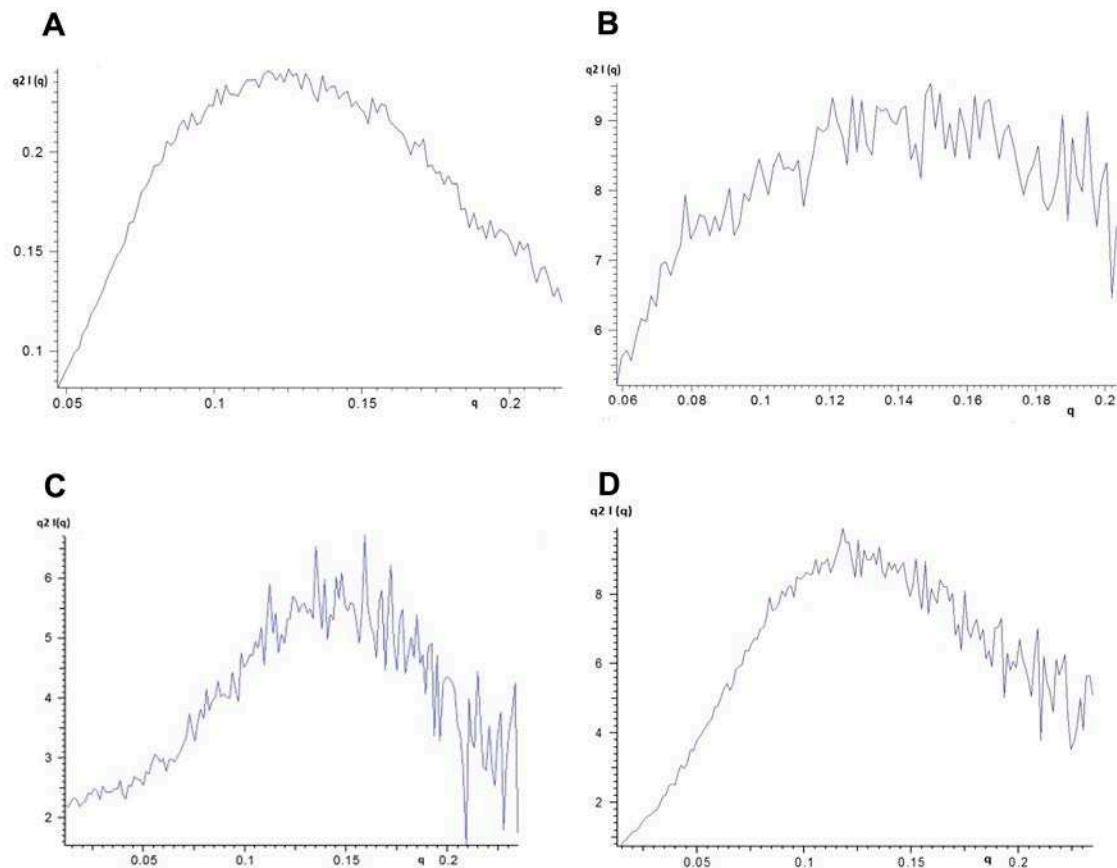compact, as at high q values, the value of $q^2 \times I(q)$ decreases and approaches zero (Figure. 8C).

Figure 8. Kratky plots of BAPKO_0422 (A), 6x-His-tagged BAPKO_0422 (B), 6x-His-tagged BB_0562 (C) 6x-His-tagged BG_0408 (D). Kratky plots obtained by Primus software (ATSAS) (Petoukhov et al., 2012) showing q2I(q) versus q (Å-1). All plots reveal the parabolic convergence for a folded particle. Lower scattering intensity at high q is indicative of compact globular folded structure with a well-defined difference between the scattering of molecule and solvent.

Molecular envelope calculation

Ab initio shape determination using dummy atoms to generate volumes whose scattering profiles fit the experimental data (Ezquerra, Garcia-Gutierrez, & Nogales, 2009) was performed using the online ATSAS package (Petoukhov et al., 2012) with default settings. DAMMIN generated 20 models, which were then aligned by DAMAVER. Outliers were removed and an average model was generated in DAMFILT. Figures were generated using PyMOL (Schrodinger, 2010) (Figures. 9, 10, 11, 12). A comparison of the SAXS data sets collected from BAPKO_0422 with and without the N-terminal His tag reveals the presence of an additional domain. This additional domain allows for the possibility of orientating the model with respect to the membrane (Figure. 13). This N-terminal domain is likely to be periplasmic (Schulz, 2000).
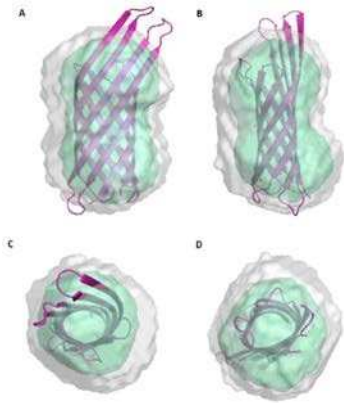
Figure 9. Molecular envelopes of 3.5 mg/ml BAPKO_0422 without the 6x-His tag. The average molecular envelope of 20 ab initio structures (grey surface) represents the dynamic motion of all atoms within BAPKO_0422. The filtered envelope (green surface) represents the most highly occupied volume and is in agreement with the shape and size of the close homologue E. coli OmpX (purple ribbon). Scattering data was collected from a solution of BAPKO_0422 at a concentration of 3.5 mg/ml in 0.3 M NaCl, 50 mM Tris-HCl, 0.1% (w/v) LDAO, 0.05% sodium azide, pH 8. A dialysis-matched buffer was used as a blank. Figure created in PyMOL (Schrodinger, 2010), using envelopes calculated by DAMAVER and DAMFILT (ATSAS) (Petoukhov et al., 2012) and coordinates of OmpX from PDB (accession code 1QJ8). a) frontal view b) side view c) top view d) bottom view.
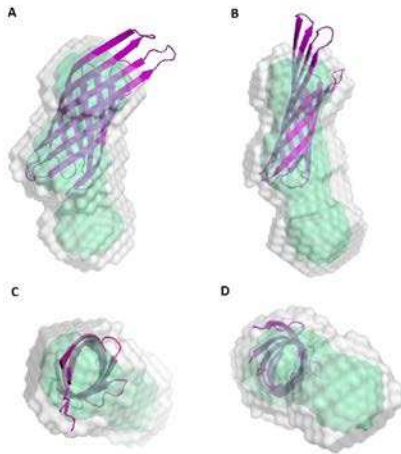

Figure 10. Molecular envelopes of 2.8 mg/ml BAPKO_0422 with the 6x-His tag. The average molecular envelope of 20 ab initio structures (grey surface) represents the dynamic motion of all atoms within BAPKO_0422. The filtered envelope (green surface) represents the most highly occupied volume and is in agreement with the shape and size of the close homologue E. coli OmpX (purple ribbon). Scattering data was collected from a solution of BAPKO_0422 at a concentration of 2.8 mg/ml in 0.3 M NaCl, 50 mM Tris-HCl, 0.1% (w/v) LDAO, 0.05% sodium azide, pH 8. A dialysis-matched buffer was used as a blank. Figure created in PyMOL (Schrodinger, 2010), using envelopes calculated by DAMAVER and DAMFLIT (ATSAS) (Petoukhov et al., 2012) and coordinates of OmpX from PDB (accession code 1QJ8). a) frontal view b) side view c) top view d) bottom view.
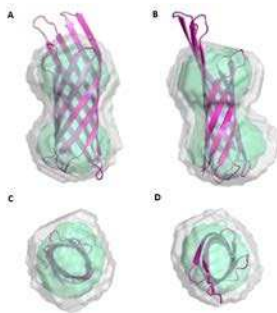

Figure 11. Molecular envelopes of 3.0 mg/ml BB_0562 with the 6x-His tag. The average molecular envelope of 20 ab initio structures (grey surface) represents the dynamic motion of all atoms within BB_0562. The filtered envelope (green surface) represents the most highly occupied volume and is in agreement with the shape and size of the close homologue E. coli OmpX (purple ribbon). Scattering data was collected from a solution of BB_0562 at a concentration of 3.0 mg/ml in 0.3 M NaCl, 50 mM Tris-HCl, 0.1% (w/v) LDAO, 0.05% sodium azide, pH 8. A dialysis-matched buffer was used as a blank. Figure created in PyMOL (Schrodinger, 2010), using envelopes calculated by DAMAVER and DAMFILT (ATSAS) (Petoukhov et al., 2012) and coordinates of OmpX from PDB (accession code 1QJ8). a) frontal view b) side view c) bottom view d) top view.
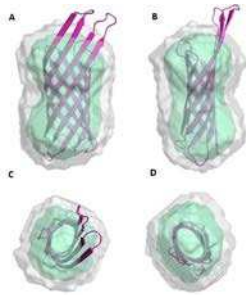
Figure 12. Molecular envelopes of 4.2 mg/ml BG_0408 with the 6x-His tag. The average molecular envelope of 20 ab initio structures (grey surface) represents the dynamic motion of all atoms within BG_0408. The filtered envelope (green surface) represents the most highly occupied volume and is in agreement with the shape and size of the close homologue E. coli OmpX (purple ribbon). Scattering data was collected from a solution of BG_0408 at a concentration of 3.0 mg/ml in 0.3 M NaCl, 50 mM Tris-HCl, 0.1% (w/v) LDAO, 0.05% sodium azide, pH 8. A dialysis-matched buffer was used as a blank. Figure created in PyMOL (Schrodinger, 2010), using envelopes calculated by DAMAVER and DAMFILT (ATSAS) (Petoukhov et al., 2012) and coordinates of OmpX from PDB (accession code 1QJ8). a) frontal view b) side view c) top view d) bottom view.
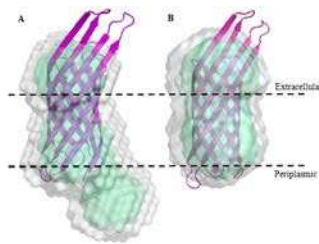

Figure 13. A comparison of molecular envelopes of BAPKO_0422 with the His tag (A) and after treatment with HRV-3C protease (B). Dashed lines indicate the approximate position of the outer membrane. The average molecular envelope of 20 ab initio structures (grey surface) represents the dynamic motion of all atoms. The filtered envelope (green surface) represents the most highly occupied volume. The purple ribbon shows E. coli OmpX (PDB accession code 1QJ8) manually orientated.Figure 13: A comparison of molecular envelopes of BAPKO_0422 with the His tag (A) and after treatment with HRV-3C protease (B). Dashed lines indicate the approximate position of the outer membrane. The average molecular envelope of 20 ab initio structures (grey surface) represents the dynamic motion of all atoms. The filtered envelope (green surface) represents the most highly occupied volume. The purple ribbon shows E. coli OmpX (PDB accession code 1QJ8) manually orientated.

Discussion

Expression and purification of recombinant proteins

pET47b(+) constructs containing BAPKO_0422, BB_0562 or BG_0408 fused to an N-terminal 6x-His tag were provided. Owing to the presence of an N-terminal signal sequence, full-length proteins may be processed by the secretory pathway resulting in membrane insertion. This may potentially influence the virulence of *E. coli* and would also negatively impact on expression yields (Yoon, Kim, & Kim, 2010). The signal sequence was therefore replaced with the 6x-His tag and HRV-3C cleavage site so that the expression would result in the formation of inclusion bodies containing the protein of interest and the translocation to the membrane would be prevented (Bannwarth & Schulz, 2003).

This tag was then enzymatically removed for the 3.5 mg/ml BAPKO_0422 sample, resulting in a native protein. The 6x-His tag and the contaminating HRV-3C were then removed by passing the material through the His-Trap HP 5 ml column: HRV-3C and the 6x-His tag remained bound and the BAPKO_0422 passed through.

HRV-3C protease is reported to cleave the HRV-3C recognition site Leu-Glu-Val-Leu-Phe-Gln/Gly-Pro with nearly 100% efficiency at a protease-to-target protein ratio of 1:100 (w/w) over 24 hours at 4°C (Cordingley, Register, Callahan, Garsky, &

Colonno, 1989). However, the ratio had to be increased to 1:10 to cleave just less than 50% of the protein over 48 hours at 4℃. It is possible that the 6x -His tag at the N-terminus of BAPKO_0422 is not easily accessible to the HRV-3C protease because the protein fold results in a decreased ability of the protease to cleave the HRV-3C recognition site.

SDS-PAGE analysis
SDS-PAGE analysis of cell lysate, soluble, insoluble and purified fractions from BAPKO_0422, BB_0562 and BG_0408 was completed to ascertain the purity of the final protein product. During SDS-PAGE analysis it has to be kept in mind that the molecular weight of a protein as determined by SDS-PAGE is only an approximation, and hence, the expected and observed molecular weight can vary (Burgess & Deutscher, 2009). This is particularly true for outer membrane proteins (Rath et al., 2009).

A large band at 45 kDa is visible in the non-induced cells, cell lysate and soluble fraction of every SDS-PAGE (Figures. 2, 3), which suggests that this is a native soluble protein from *E. coli*. The molecular weight of BG_0408 is 22.8 kDa (Table 3). Two bands at approximately 20 and 38 kDa in the insoluble fraction and three bands at 60, 150 and 250 kDa in the purified fraction are the most prominent (Figure. 2). BG_0408 contains two cysteines (Table 2) that are likely to form disulphide bonds in a non-reduced environment. The 20 kDa band in the insoluble fraction is likely to be a BG_0408 monomer. The band at 38 kDa could be a contamination or a dimer. Proteins in the insoluble fraction are solubilised in 8 M urea and should therefore be denatured; however, after the addition of water and NuPAGE LDS Sample Buffer the concentration of urea halved. As no reducing agent is present in the insoluble fraction, disulphide bonds are to be expected. This, coupled with the fact that SDS-induced oligomerisation of proteins has also been reported (Watt et al., 2013) and that the molecular weight corresponds to a dimer, indicates that the 38 kDa band is, indeed, a BG_0408 dimer.

The 60, 150 and 250 kDa bands in the purified fraction could represent a multimeric state of the protein. The sample at this stage is expected to be relatively pure and concentrated. BG_0408 monomers will, therefore, come into closer contact with each other, allowing the formation of oligomers. Since the native oligomeric state of this protein is not known, it is possible that BG_0408 naturally forms oligomers in the *Borrelial* outer membrane. This could be confirmed using a Western blot targeting the 6x-His tag with the anti-His tag antibody. SDS-PAGE with a large concentration of reducing agent such as DTT could also confirm whether the multiple bands are the result of oligomerisation or contamination. BAPKO_0422 has also been shown to dimerise at high concentrations (Gemma Brown, 2014). This dimerisation was confirmed by Western blotting and was not dependent on disulphide bonds. Therefore, it is possible that there is some physiological relevance to this dimerisation, and this will require further study.

BB_0562 has an expected molecular weight of 20.2 kDa (Table 2). The purified fraction shows a band at approximately 20 kDa. There is a less prominent band at 18 kDa which could be caused either by degradation or by contamination. Many bands are visible in the insoluble fraction, suggesting a higher amount of contamination before the final purification step in comparison to BG_0408 (Figure. 3)

or BAPKO_0422 (Dyer et al., 2015). The purified fraction of BAPKO_0422 (Dyer et al., 2015) shows a single prominent band at 23 kDa, which is in agreement with the expected molecular weight (Table 2).

Analysis of SAXS data
SAXS plays a fundamental role in the investigation of macromolecular structures in solution. The structure of native proteins can be studied in near physiological environments and structural changes in response to various external conditions can be analysed (Koch, Vachette, & Svergun, 2003). SAXS measures the difference in scattering between the macromolecule and buffer; data from a solution of monodisperse protein can therefore provide the overall shape of a molecule (Burke & Butcher, 2012). The size of the scattering object in solution can be determined using the radius of gyration (Receveur-Brechot & Durand, 2012).

OmpX is a single-domain 8-stranded β-barrel protein with the molecular weight of 18 kDa (Vogt & Schulz, 1999), and shares a sequence homology with BAPKO_0422 (Dyer et al., 2015). OmpX was therefore used as a guide molecule and the calculated molecular envelopes of BAPKO_0422, BB_0562 and BG_0408 were compared to the known structure of OmpX.

SAXS data were collected from solutions of BAPKO_0422 at two different concentrations (3.5 and 2.8 mg/ml), BB_0562 (3 mg/ml) and BG_0408 (4.2 mg/ml). Linear Guinier plots (Figure. 6) indicate that all samples are monodisperse (Svergun, Koch, Timmins, & May, 2013). Radius of gyration values were calculated by Guinier analysis, GNOM fit (reciprocal space) and *P(r)* plot (real space) (Table 3). All values are in agreement, but R_g can be calculated more accurately by GNOM from the *P(r)* function, which contains the whole dataset, rather than from the slope of a small region of data points from a Guinier plot (Jacques & Trewhella, 2010). The R_g values are comparable to that of OmpX (18.20 Å, calculated using OmpX PDB file accession code 1QJ8, using filters for globular protein evaluation software (Jayaram, 2009)), suggesting that all proteins are monomeric within the tested environment. This is in contrast to the multimers seen on the SDS-PAGE for BG_0408, and may be due to the higher concentrations of reducing agent added to SAXS samples.

The pair-distance distribution function (*P(r)* function) was obtained through a Fourier transform of the raw scattering data (Jacques & Trewhella, 2010) and provides information on the overall shape of a molecule by describing the paired-set of all distances between points in an object (Svergun et al., 2013). The single smooth bell-shaped curves (Figures. 7A, 7B, 7C, 7D) indicate that BAPKO_0422, BB_0562 and BG_0408 are single-domain globular proteins. The extended tails of 3.5 mg/ml BAPKO_0422, BB_0562 and BG_0408 (Figures. 7A, 7C and 7D) show an elongated structure consistent with a cylindrical-shaped molecule with no aggregation or interparticle interference (Jacques & Trewhella, 2010). The bell-shaped curve of 2.8 mg/ml BAPKO_0422 (Figure. 5) does not approach zero with a steady slope, which could be indicative of particle overlap potentially caused by the flexible 6x-His tag at the N-terminus (Jacques & Trewhella, 2010). The points at which the *P(r)* function returns to zero indicates a maximum length of 39 Å for BB_0562 (Figure. 7C), 46 Å for BG_0408 (Figure. 7D), 45 Å for BAPKO_0422 without the 6x-His tag (Figure. 7A) and 46 Å for the BAPKO_0422 with the 6x-His tag (Figure. 7B). BAPKO_0422 without the 6x-His tag is expected to be a more compact molecule.

Kratky plots of BAPKO_0422 (Figures. 8A, 8B), BB_0562 (Figure. 8C) and BG_0408 (Figure. 8D) revealed the parabolic convergence for a folded particle. The clear peaks and decreasing scattering intensity at high q indicates a compact globular folded structure with a well-defined difference between the scattering of molecule and solvent (Glatter & Kratky, 1982). A small degree of disorder was present in Kratky plots of BAPKO_0422 and BG_0408 (Figure. 8).

Molecular envelope calculation
Ab initio shape determination using dummy atoms to generate volumes whose scattering profiles fit the experimental data (Ezquerra et al., 2009) was performed using the online ATSAS package (Petoukhov et al., 2012). For the correct background subtraction it is important to use a carefully matched blank (Svergun et al., 2013); hence, dialysis-matched buffer with the exact concentration of LDAO as in the sample was used.

The average molecular envelope of 20 *ab initio* structures (grey surface) represents the dynamic motion of all atoms within the BAPKO_0422 (Figures 9 and 10), BB_0562 (Figure. 11) and BG_0408 (Figure. 12). The filtered envelope (green surface) represents the most greatly occupied volume. All filtered envelopes (Figures. 9, 10, 11 and 12) are consistent with an 8-stranded β-barrel and are in agreement with the shape and size of the *E. coli* homologue OmpX (purple ribbon) with only the loop regions protruding outwards. As the loop regions are flexible, the molecular envelope accounts for an average of positions. When the molecular and filtered envelopes are generated in PyMOL (Schrodinger, 2010) as spheres rather than surface, the size of the filtered envelope matches that of the OmpX.

The N-terminal 6x-His tag is expected to be located at the perisplasmic side of the proteins (Schulz, 2000). Molecular envelopes of BAPKO_0422 with (Figure. 10) and without (Figure. 9) the 6x-His tag were compared to establish the orientation of the molecule (Figure 13). BAPKO_0422 with the 6x-His tag (Figures. 10, 13) shows three regions with higher flexibility within the molecule, which are likely to be the external loops, periplasmic turns and the His tag. Periplasmic turns are shorter than loops (Schulz, 2000) and are therefore expected to produce smaller flexible regions within the molecules, which may provide some information about the orientation of the BAPKO_0422 without the 6x-His tag (Figure. 9). The His tag is fairly small in comparison to turns and loops; hence, the smallest flexible region was expected to be oriented towards the periplasmic side (Figure. 13). However, it was not possible to determine the periplasmic and external side of the BAPKO_0422 after the enzymatic digest with HRV-3C protease (Figure. 9, 13), BB_0562 (Figure. 11) and BG_0408 (Figure. 12), as the flexible regions are of a similar size.

Numerous questions arise from this work, such as the nature of the BG_0408 dimers observed during SDS-PAGE and why this does not match the monomeric structure from SAXS. If a possible contamination is excluded by a Western blot, the potential physiological relevance of such oligomerisation needs to be investigated. Size exclusion chromatography could help to determine the oligomeric state of BG_0408 in a solution.

To produce a statistically significant data set, the SAXS data for BAPKO_0422, BB_0562 and BG_0408 need to be collected in triplicate from solutions of various concentrations. The orientation of the BAPKO_0422 without the His tag, BB_0562 and BG_0408 β-barrels also remain to be determined. The His tag of BB_0562 and BG_0408 could be enzymatically removed, and a visual comparison of the molecular envelopes may produce the necessary information. Alternatively, partial trypsin digest followed by mass spectrometry could help to identify flexible loop regions and possibly the orientation in the membrane. Ultimately, X-ray crystallography will provide high-resolution structures of these β-barrels.

The function of BAPKO_0422, BB_0562 and BG_0408 is currently not known. It is postulated that BAPKO_0422 and BG_0408 could play a role in host immune evasion as their binding to human factor H has been recently shown (Dyer et al., 2015). Similar experiments need to be performed for BB_0562 in order to provide an insight into its function.

Conclusion
Three proteins from the outer membrane of *Borrelia* (BAPKO_0422, BB_0562 and BG_0408) were successfully produced using the *E. coli* recombinant expression system. Theoretical predictions suggested that these proteins form 8-stranded membrane-spanning β-barrels. Data from SAXS is consistent with this hypothesis. Molecular envelopes determined *ab initio* closely resemble the crystal structure of homologous OmpX. All the proteins studied are single-domain cylindrical-shaped molecules with no evidence of an internal pore.

The function of these proteins remains to be determined. The functional variety of β-barrels in an outer membrane is highlighted in Table 1. Recently, BAPKO_0422 and BG_0408 have been shown to bind human factor H (Dyer et al., 2015) and could, therefore, act as a mediators of bacteria-host adhesion and form part of a bacterial defence against the complement immune response.

The work presented here emphasises the important fact that numerous proteins on the surface of *Borrelia* remain to be characterised, both structurally and functionally. A complete annotation of integral membrane proteins is crucial to understand the wide range of possible host–pathogen interactions and to aid vaccine and drug development.

References

Auwaerter, P. G., Aucott, J., & Dumler, J. S. (2004). Lyme borreliosis (Lyme disease): molecular and cellular pathobiology and prospects for prevention, diagnosis and treatment. *Expert Reviews in Molecular Medicine, 6*(2), 1–22. http://dx.doi.org/10.1017/S1462399404007276

Bannwarth, M., & Schulz, G. E. (2003). The expression of outer membrane proteins for crystallization. *Biochimica et Biophysica Acta, 1610*(1), 37–45. http://dx.doi.org/10.1016/S0005-2736(02)00711-3

Barbour, A. G. (1998). Fall and rise of Lyme disease and other Ixodes tick-borne infections in North America and Europe. *British Medical Bulletin, 54*(3), 647–658. Retrieved from http://bmb.oxfordjournals.org/content/54/3/647.abstract

Barbour, A. G., & Hayes, S. F. (1986). Biology of Borrelia species. *Microbiological Reviews, 50*(4), 381–400.

Biesiada, G., Czepiel, J., Lesniak, M. R., Garlicki, A., & Mach, T. (2012). Lyme disease: review. *Archives of Medical Science, 8*(6), 978–982. http://dx.doi.org/10.5114/aoms.2012.30948

Bunikis, I., Denker, K., Östberg, Y., Andersen, C., Benz, R., Bergström, S., . . . Medicinska, F. (2008). An RND-type efflux system in Borrelia burgdorferi is involved in virulence and resistance to antimicrobial compounds. *PLoS Pathogens, 4*(2), e1000009. http://dx.doi.org/10.1371/journal.ppat.1000009

Burgess, R. R., & Deutscher, M. P. (2009). *Guide to protein purification* (2nd ed.). Amsterdam, Netherlands, and Boston: Elsevier/Academic Press.

Burke, J. E., & Butcher, S. E. (2012). Nucleic acid structure characterization by small angle X-ray scattering (SAXS). *Current protocols in nucleic acid chemistry, CHAPTER 7*, Unit 7.18–Unit 17.18. http://dx.doi.org/10.1002/0471142700.nc0718s51

Cordingley, M. G., Register, R. B., Callahan, P. L., Garsky, V. M., & Colonno, R. J. (1989). Cleavage of small peptides in vitro by human rhinovirus 14 3C protease expressed in Escherichia coli. *Journal of Virology, 63*(12), 5037–5045.

Cullen, P. A., Haake, D. A., & Adler, B. (2004). Outer membrane proteins of pathogenic spirochetes. *FEMS Microbiology Reviews,* 28(3), 291–318.

Dyer, A., Brown, G., Stejskal, L., Laity, P. R. Bingham, R. J. (2015) The Borrelia afzelii outer membrane protein BAPKO_0422 binds human factor-H and is predicted to form a membrane-spanning β-barrel. *Bioscience Reports, 35*(4),e00240. http://dx.doi.org/10.1042/BSR20150095

Ezquerra, T. A., Garcia-Gutierrez, M. C., Nogales, A., & Gomez, M. (2009). *Applications of Synchrotron Light to Scattering and Diffraction in Materials and Life Sciences.* Berlin and Heidelberg: Springer-Verlag.

Fernández, C., Hilty, C., Bonjour, S., Adeishvili, K., Pervushin, K., & Wüthrich, K. (2001). Solution NMR studies of the integral membrane proteins OmpX and OmpA from Escherichia coli. *FEBS Letters, 504*, 173–178. http://dx.doi.org/10.1016/S0014-5793(01)02742-9

Freeman, T. C., Jr., Landry, S. J., & Wimley, W. C. (2011). The prediction and characterization of YshA, an unknown outer-membrane protein from Salmonella

typhimurium. *Biochimica et Biophysica Acta, 1808*(1), 287–297. http://dx.doi.org/10.1016/j.bbamem.2010.09.008

Glatter, O., & Kratky, O. (1982). *Small Angle X-ray Scattering*. London: Academic Press.

Hayat, S., & Elofsson, A. (2012). Ranking models of transmembrane beta-barrel proteins using Z-coordinate predictions. *Bioinformatics, 28*(12), i90–96. http://dx.doi.org/10.1093/bioinformatics/bts233

Hong, H., Patel, D. R., Tamm, L. K., & Van Den Berg, B. (2006). The outer membrane protein OmpW forms an eight-stranded β-barrel with a hydrophobic channel. *Journal of Biological Chemistry, 281*(11), 7568–7577. http://dx.doi.org/10.1074/jbc.M512365200

Jacques, D. A., & Trewhella, J. (2010). Small-angle scattering for structural biology–expanding the frontier while avoiding the pitfalls. *Protein Science, 19*(4), 642–657. http://dx.doi.org/10.1002/pro.351

Jayaram, B. (2009). *Filters for Globular Protein Evaluation*. Retrieved from http://www.scfbio-iitd.res.in/bioinformatics/bioinformaticssoftware.htm

Kenedy, M. R., Luthra, A., Anand, A., Dunn, J. P., Radolf, J. D., & Akins, D. R. (2014). Structural modeling and physicochemical characterization provide evidence that P66 forms a β-barrel in the Borrelia burgdorferi outer membrane. *Journal of Bacteriology, 196*(4), 859–872. http://dx.doi.org/10.1128/JB.01236-13

Koch, M. H., Vachette, P., & Svergun, D. I. (2003). Small-angle scattering: a view on the properties, structures and structural changes of biological macromolecules in solution. *Quarterly Reviews of Biophysics, 36*(2), 147–227.

Kudryashev, M., Cyrklaff, M., Wallich, R., Baumeister, W., & Frischknecht, F. (2010). Distinct in situ structures of the Borrelia flagellar motor. *Journal of Structural Biology, 169*(1), 54–61. http://dx.doi.org/10.1016/j.jsb.2009.08.008

LaRocca, T. J., Crowley, J. T., Cusack, B. J., Pathak, P., Benach, J., London, E., . . . Benach, J. L. (2010). Cholesterol lipids of Borrelia burgdorferi form lipid rafts and are required for the bactericidal activity of a complement-independent antibody. *Cell Host & Microbe, 8*(4), 331–342. http://dx.doi.org/10.1016/j.chom.2010.09.001

LaRocca, T. J., Pathak, P., Chiantia, S., Toledo, A., Silvius, J. R., Benach, J. L., & London, E. (2013). Proving lipid rafts exist: membrane domains in the prokaryote Borrelia burgdorferi have the same properties as eukaryotic lipid rafts. *PLoS Pathogens, 9*(5), e1003353. http://dx.doi.org/10.1371/journal.ppat.1003353

Lenhart, T. R., & Akins, D. R. (2010). Borrelia burgdorferi locus BB0795 encodes a BamA orthologue required for growth and efficient localization of outer membrane

proteins. *Molecular Microbiology, 75*(3), 692–709. http://dx.doi.org/10.1111/j.1365-2958.2009.07015.x

Lindgren, E., & Jaenson, T. G. T. (2006). Lyme borreliosis in Europe: influences of climate and climate change, epidemiology, ecology and adaptation measures In B. Menne & K. L. Ebi (Eds.), *Climate change and adaptation: strategies for human health*. (pp. 157–188). Darmstadt: WHO, Steinkopff Verlag.

Maurya, S. R., & Mahalakshmi, R. (2013). Modulation of human mitochondrial voltage-dependent anion channel 2 (hVDAC-2) structural stability by cysteine-assisted barrel-lipid interactions. *Journal of Biological Chemistry, 288*(35), 25584–25592. http://dx.doi.org/10.1074/jbc.M113.493692

Murzin, A. G., Lesk, A. M., & Chothia, C. (1994). Principles determining the structure of beta-sheet barrels in proteins. II. The observed structures. *Journal of Molecular Biology, 236*(5), 1382–1400.

Noinaj, N., Kuszak, A. J., Gumbart, J. C., Lukacik, P., Chang, H., Easley, N. C., . . . Buchanan, S. K. (2013). Structural insight into the biogenesis of β-barrel membrane proteins. *Nature, 501*(7467), 385–390. http://dx.doi.org/10.1038/nature12521

Paster, B. J., Dewhirst, F. E., Weisburg, W. G., Tordoff, L. A., Fraser, G. J., Hespell, R. B., . . . Woese, C. R. (1991). Phylogenetic analysis of the spirochetes. *Journal of Bacteriology, 173*(19), 6101–6109.

Pautsch, A., & Schulz, G. E. (2000). High-resolution structure of the OmpA membrane domain. *Journal of Molecular Biology, 298*(2), 273–282. http://dx.doi.org/10.1006/jmbi.2000.3671

Petoukhov, M. V., Franke, D., Shkumatov, A. V., Tria, G., Kikhney, A. G., Gajda, M., . . . Svergun, D. I. (2012). New developments in the program package for small-angle scattering data analysis. *Journal of Applied Crystallography, 45*(Pt 2), 342–350. http://dx.doi.org/10.1107/S0021889812007662

Pilsl, H., Smajs, D., & Braun, V. (1999). Characterization of Colicin S4 and Its Receptor, OmpW, a Minor Protein of the Escherichia coli Outer Membrane. *Journal of Bacteriology, 181*(11), 3578–3581.

Prasadarao, N. V., Wass, C. A., Weiser, J. N., Stins, M. F., Huang, S. H., & Kim, K. S. (1996). Outer membrane protein A of Escherichia coli contributes to invasion of brain microvascular endothelial cells. *Infection and Immunity, 64*(1), 146–153.

Radolf, J. D., Caimano, M. J., Stevenson, B., & Hu, L. T. (2012). Of ticks, mice and men: understanding the dual-host lifestyle of Lyme disease spirochaetes. *Nature Reviews Microbiology, 10*(2), 87–99. http://dx.doi.org/10.1038/nrmicro2714

Radolf, J. D., Robinson, E. J., Bourell, K. W., Akins, D. R., Porcella, S. F., Weigel, L. M., . . . Norgard, M. V. (1995). Characterization of outer membranes isolated from

Treponema pallidum, the syphilis spirochete. *Infection and Immunity, 63*(11), 4244–4252.

Rath, A., Glibowicka, M., Nadeau, V. G., Chen, G., Deber, C. M., & Engelman, D. M. (2009). Detergent Binding Explains Anomalous SDS-Page Migration of Membrane Proteins. *Proceedings of the National Academy of Sciences of the United States of America, 106*(6), 1760–1765. http://dx.doi.org/10.1073/pnas.0813167106

Receveur-Brechot, V., & Durand, D. (2012). How random are intrinsically disordered proteins? A small angle scattering perspective. *Current Protein & Peptide Science, 13*(1), 55–75.

Rudenko, N., Golovchenko, M., Belfiore, N. M., Grubhoffer, L., & Oliver, J. J. H. (2014). Divergence of Borrelia burgdorferi sensu lato spirochetes could be driven by the host: diversity of Borrelia strains isolated from ticks feeding on a single bird. *Parasites & Vectors, 7*(1), 4. http://dx.doi.org/10.1186/1756-3305-7-4

Schrodinger LLC. (2010). *The PyMOL Molecular Graphics System*, Version 1.3r1.

Schulz, G. E. (2000). beta-Barrel membrane proteins. *Current Opinion in Structural Biology, 10*(4), 443–447.

Seemanapalli, S. V., Xu, Q., McShan, K., & Liang, F. T. (2010). Outer surface protein C is a dissemination-facilitating factor of Borrelia burgdorferi during mammalian infection. *PLoS One, 5*(12), e15830. http://dx.doi.org/10.1371/journal.pone.0015830

Smith, S. G. J., Mahon, V., Lambert, M. A., & Fagan, R. P. (2007). A molecular Swiss army knife: OmpA structure, function and expression. *FEMS Microbiology Letters, 273*(1), 1–11. http://dx.doi.org/10.1111/j.1574-6968.2007.00778.x

Stanek, G., Fingerle, V., Hunfeld, K. P., Jaulhac, B., Kaiser, R., Krause, A., . . . Lund, U. (2011). Lyme borreliosis: Clinical case definitions for diagnosis and management in Europe. *Clinical Microbiology and Infection, 17*(1), 69–79. http://dx.doi.org/10.1111/j.1469-0691.2010.03175.x

Steere, A. C. (2001). Lyme disease. *New England Journal of Medicine, 345*(2), 115–125. http://dx.doi.org/10.1056/NEJM200107123450207

Steere, A. C., Coburn, J., & Glickstein, L. (2004). The emergence of Lyme disease. *Journal of Clinical Investigation, 113*(8), 1093–1101. http://dx.doi.org/10.1172/JCI21681

Svergun, D. I., Koch, M. H. J., Timmins, P. A., & May, R. P. (2013). *Small Angle X-ray and Neutron Scattering from Solutions of Biological Macromolecules*. New York: Oxford University Press.

Tamm, L. K., Hong, H., & Liang, B. (2004). Folding and assembly of beta-barrel membrane proteins. *Biochimica et Biophysica Acta, 1666*(1–2), 250–263. http://dx.doi.org/10.1016/j.bbamem.2004.06.011

Templeton, T. J. (2004). Borrelia outer membrane surface proteins and transmission through the tick. *Journal of Experimental Medicine, 199*(5), 603–606. http://dx.doi.org/10.1084/jem.20040033

The UniProt Consortium. (2015). UniProt: a hub for protein information. *Nucleic Acids Research, 43*, D204–D212. http://dx.doi.org/10.1093/nar/gku989

Thein, M., Bonde, M., Bunikis, I., Denker, K., Sickmann, A., Bergström, S., . . . Medicinska, F. (2012). DipA, a pore-forming protein in the outer membrane of lyme disease spirochetes exhibits specificity for the permeation of dicarboxylates. *PLoS One, 7*(5), e36523. http://dx.doi.org/10.1371/journal.pone.0036523

Vogt, J., & Schulz, G. E. (1999). The structure of the outer membrane protein OmpX from Escherichia coli reveals possible mechanisms of virulence. *Structure, 7*(10), 1301–1309. http://dx.doi.org/10.1016/S0969-2126(00)80063-5

Wang, Y. (2002). The Function of OmpA in Escherichia coli. *Biochemical and Biophysical Research Communications, 292*(2), 396–401. http://dx.doi.org/10.1006/bbrc.2002.6657

Watt, A. D., Perez, K. A., Rembach, A., Sherrat, N. A., Hung, L. W., Johanssen, T., . . . Barnham, K. J. (2013). Oligomers, fact or artefact? SDS-PAGE induces dimerization of β-amyloid in human brain samples. *Acta Neuropathologica, 125*(4), 549–564. http://dx.doi.org/10.1007/s00401-013-1083-z

Wu, X.-B., Tian, L.-H., Zou, H.-J., Wang, C.-Y., Yu, Z.-Q., Tang, C.-H., . . . Pan, J.-Y. (2013). Outer membrane protein OmpW of Escherichia coli is required for resistance to phagocytosis. *Research in Microbiology, 164*(8), 848–855. http://dx.doi.org/10.1016/j.resmic.2013.06.008

Yoon, S. H., Kim, S. K., & Kim, J. F. (2010). Secretory production of recombinant proteins in Escherichia coli. *Recent Patents on Biotechnology, 4*(1), 23-29